Unveiling the Mechanisms Leading to H_2 Production Promoted by Water Decomposition on Epitaxial graphene at Room Temperature

A. Politano[1,*], M. Cattelan[2], D.W. Boukhvalov[3,4,*], D. Campi[5,‡], A. Cupolillo[1], S. Agnoli[2], N.G. Apostol[6,§], P. Lacovig[6], S. Lizzit[6], D. Farías[7], G. Chiarello[1], G. Granozzi[2], and R. Larciprete[8]
[1] Department of Physics, University of Calabria, via ponte Bucci, 31/C, I-87036 Rende (CS), Italy
[2] Department of Chemical Sciences, University of Padova, via Marzolo 1, I-35131 Padova, Italy
[3] Department of Chemistry, Hanyang University, 17 Haengdang-dong, Seongdong-gu, Seoul 133-791, South Korea
[4] Theoretical Physics and Applied Mathematics Department, Ural Federal University, Mira Street 19, 620002 Ekaterinburg, Russia
[5] Department of Materials Science, University of Milano-Bicocca, Via R. Cozzi 55, I-20125, Milano, Italy
[6] Elettra-Sincrotrone Trieste S.C.p.A., S.S. 14, Km 163.5, I-34149 Trieste, Italy
[7] Departamento de Física de la Materia Condensada & Instituto de Ciencia de Materiales "Nicolás Cabrera" & Condensed Matter Physics Center (IFIMAC), Universidad Autónoma de Madrid, 28049 Madrid, Spain
[8] CNR, Institute for Complex Systems, Via Fosso del Cavaliere 100, I-00133 Roma, Italy
‡ Present address: Theory and Simulation of Materials (THEOS), and National Centre for Computational Design and Discovery of Novel Materials (MARVEL), Ecole Polytechnique Fédérale de Lausanne, 1015 Lausanne, Switzerland
§ Present address: National Institute of Materials Physics, Atomistilor 105b, 077125 Magurele-Ilfov, Romania.

ABSTRACT

By means of a combination of surface-science spectroscopies and theory, we investigate the mechanisms ruling the catalytic role of epitaxial graphene (Gr) grown on transition-metal substrates for the production of hydrogen from water. Water decomposition at the Gr/metal interface at room temperature provides a hydrogenated Gr sheet, which is buckled and decoupled from the metal substrate. We evaluate the performance of Gr/metal interface as a hydrogen storage medium, with a storage density in the Gr sheet comparable with state-of-the-art materials (1.42 wt.%). Moreover, thermal programmed reaction experiments show that molecular hydrogen can be released upon

heating the water-exposed Gr/metal interface above 400 K. The Gr hydro/dehydrogenation process might be exploited for an effective and eco-friendly device to produce (and store) hydrogen from water, i.e. starting from an almost unlimited source.

*corresponding authors: DWB (danil@hanyang.ac.kr) and AP (antonio.politano@fis.unical.it).

Keywords: graphene; water; hydrogen storage; hydrogen production

Introduction

Hydrogen represents an alternative eco-friendly and sustainable energy carrier capable of answering the increasing global energy demand.[1-5] The hydrogen economy covers three functional areas: production, storage, and usage. Currently, hydrogen is mainly produced from natural gas *via* steam reforming [6]. Sustainable alternatives include biological [7] or catalytic [8] degradation of biomass [9] and electrochemical [10] or photochemical water splitting. [11-14] However, some of these processes are unsustainable, since they require a considerable amount of unrenewable energy consumption. For a diffuse usage, energy devices must be compact, [15] combining both fuel production/storage and conversion of primary energy sources into the energy service. A smart solution could be represented by a unique material active for both the production and the storage of hydrogen. Gr is a promising solid-state material for hydrogen storage,[16-18] alternative to metal hydrides[19] and metal-organic frameworks [20, 21] designed to overcome the restrictions of state-of-the-art technologies for hydrogen storage in tanks.[20] An important challenge is represented by the eco-friendly, economic and effective production of clean H_2 fuels from Gr.[16] _ENREF_16

Herein, we elucidate the mechanisms which allow the exploitation of Gr/transition-metal interfaces for the production and storage of hydrogen from water. Our model system is Gr/Ni(111) and we adopt both advanced spectroscopic tools and density functional theory (DFT) to clarify the various reaction steps leading to water dissociation at room temperature (RT), whose mechanism is still unclear, [22, 23] and to the subsequent hydrogen production.

Results and Discussion

The modification of the Gr/Ni(111) interface after the exposure to water at RT has been explored by means of high-resolution X-ray photoelectron spectroscopy (XPS) with synchrotron radiation. The XPS C1s spectrum measured on pristine Gr on Ni(111) (Figure 1a, top) reveals a dominating (C_0, 284.84 eV) and a weaker (C_1, 284.39 eV) components, assigned to strongly interacting and weakly interacting (in correspondence of rotated domains) Gr on Ni(111),[24] respectively, and/or to the coexistence of top-fcc and bridge-top domains in Gr/Ni(111), [25] plus a minimal additional contribution of Ni carbide[26] (C_2, 283.27 eV).

The exposure of Gr to 10^6 L (1 L=$1.33 \cdot 10^{-6}$ mbar·s) of water at RT strongly modifies the C 1s line-shape (Figure 1a, bottom): the intensity of the originally dominant peak C_0 decreases, the C_1 peak disappears and the new components C_3, C_4 and C_5 emerge at 284.08, 285.30 and 284.31 eV, respectively. C_3 and C_4 are the spectral features observed after the hydrogenation of Gr/Ni(111), [27] whereas, as it will be clear below, C_5 accounts for the Gr regions decoupled from the substrate by water intercalation.

Further information on the water dosed-Gr/Ni(111) interface is obtained by the analysis of the O 1s core-level spectrum (Figure 1b), which shows a main component at 532.51 (O_1) and a second feature at 530.54 eV (O_2). On the basis of results reported in Ref. 28, we assign the two components to undissociated water molecules and to hydroxyl species coming from water dissociation, respectively. It is worth noting that the relative intensity of H_2O and OH components is strongly influenced by the interface configuration. Lacking any information about the arrangement of the water molecules below Gr, also in relation to the localization of the OH groups, the estimation of the amount of intercalated water and of the percentage of dissociated molecules from the O 1s component intensities might be misleading .

Significant water-induced effects are also evident in the valence-band spectra shown in Figure 1c. The pristine Gr/Ni(111) is characterized by three features: the intense peak at 1.35 eV is ascribed to Ni 3d bands, while two broad features centered around 6.3 and 9.3 eV are related to $\sigma_{2,3v}$ and π_{1v}

valence-band Gr-derived states, respectively. [29] The strong hybridization between $\sigma_{2,3v}$ and π_{1v} states and Ni 3d band induces a binding-energy difference of ~2.4 and ~1 eV, respectively, compared to the corresponding states in graphite. [29] Conversely, the spectrum acquired after water exposure exhibits a band associated to the H_2O-$3a_1$ state at ~7 eV. [30] The attenuated intensity of the valence band in the water-exposed Gr/Ni(111) is due to the presence of chemisorbed species.

To define the configuration of the water-dosed interface, it should be noted that the lack in the C 1s spectrum of spectral features assignable to C-OH bonds, which should arise at ~ 286.5 eV, [31] indicates that the hydroxyl groups are bonded to the Ni substrate. On the other hand, the undissociated water molecules, which do not stick to defect-free Gr nor adsorb on the Ni(111) surface at RT, could be trapped at Gr defect sites or intercalated underneath the Gr cover.

Valuable information about the configuration of surface chemical bonds is provided by the investigation of surface vibrations with high-resolution electron energy loss spectroscopy (HREELS). The vibrational spectrum of H_2O-dosed Gr/Ni(111), shown at the bottom of Figure 1d, exhibits the C-H bending and stretching modes at 179 and 367 meV,[32] respectively. The absence of C-OH and O-H vibrations at 65-75 and 410-460 meV, [33] respectively, confirms that the OH groups arising from water dissociation are not bound to Gr, which only forms bonds with H atoms. It should be noticed that OH-Ni vibrational modes underneath the Gr cover cannot be probed by the HREELS technique.[34] Similarly, the absence in the vibrational spectra of modes coming from undissociated water molecules (for H_2O vibrational spectrum, see Figure S4 in the Supporting Information, SI) demonstrates that the H_2O molecules, detected in the O 1s spectrum in Figure 1b, have penetrated below Gr.

Therefore, the scenario emerging from our results is that water molecules interacting with the Gr/Ni(111) interface intercalate below Gr and partly dissociate, leading to H atoms bonded to Gr and OH groups bonded to the metal substrate. This is expected to result into an increased Gr-Ni distance and into the buckling of the Gr sheet (see Figure 3 and its description), as a consequence of the hydrogenation-induced modification in the hybridization from sp^2 to sp^3.[35] Accordingly, the DFT calculations of core-level shifts for C 1s for Gr decoupled from the Ni substrate by the presence of

intercalated species indicate a notable down-shift of ~0.7 eV (see Figure S6 in the SI), in agreement with the behavior observed in Figure 1a.

The thermal stability of the water-dosed Gr/Ni(111) interface was probed by monitoring the C 1s spectra by means of fast-XPS experiments performed in real time during sample heating. The sequence of C 1s spectra is shown as a 2D plot in Figure 2a, whereas Figure 2b reports the intensity of the different C 1s spectral components. Thermal annealing at 350 K starts to convert C_3 and C_4 into C_0. In the high-resolution C 1s spectrum taken on the sample heated at 470 K (see Figure S5 in the SI) C_3 has vanished ; C_0 and C_1 have recovered most of their initial intensity after complete hydrogen desorption; whereas the extra intensity at ~ 284.3 eV in correspondence of C_5 still reveals the presence of intercalated water. After annealing to 770 K, the C 1s spectrum has fully recovered the line-shape and intensity of the pristine Gr on Ni(111). The C 1s spectra measured on Gr/Ni(111) before exposure to water and after sample heating of the water-dosed system are compared in the inset of Figure 2b. Their perfect similarity leads us to conclude that the Gr hydro/dehydrogenation process does not induce any structural damage of the Gr lattice. It is worth noting that, whereas defected Gr/Ru(0001) exposed to water is dramatically split, defect-free Gr remains intact, and Gr/Cu(111) is only occasionally damaged.[36] Accordingly, our results demonstrate the stability of Gr/Ni(111) exposed to water and the perfect process reversibility.

A similar evolution of the water-dosed Gr/Ni(111) interface with the temperature is illustrated by HREELS spectra (Figure 2c), which show that above 300 K the intensity of C-H vibrations decreases progressively and finally vanishes at ~440 K. In the thermal evolution of the O 1s spectrum (Figure 2d), the behavior of the intensity of O_1 and O_2 components (defined in Figure 1b) indicates a different evolution for the OH and H_2O species present at the Gr/Ni(111) interface. The progressive decrease of the O_1 component, which starts at 400 K and proceeds up to 700 K, in parallel with the C_5 component of the C 1s spectrum, confirms that the H_2O molecules are entrapped underneath the Gr cover. The increasing temperature allows them to diffuse and desorb, likely passing through grain

boundaries and defects of the Gr lattice. By contrast, the constant intensity of the O_2 peak ascribed to OH groups attests the higher thermal stability up to 750 K of the OH-Ni bonds.

The various physicochemical processes involving water intercalated underneath Gr were modelled by DFT calculations (Figure 3). Grain boundaries are the main route for the penetration of water between Gr and the metal substrates in agreement with the results reported for the intercalation of atoms[37] and molecules[38] below Gr. Water intercalation at RT requires high partial pressure (i.e. ~10^{-3} mbar, see Methods), as also found for CO intercalation at RT in Gr/metals.[39, 40] The next step of our DFT survey is the modelling of H_2O decomposition at the Gr/metal interface. We considered the decomposition of two water molecules, which can occur through different paths, leading to the following possible configurations: (*a*) two H atoms adsorbed on Gr and two OH groups on the metal substrate (Figure 3b); (*b*) both OH groups on Gr and both H atoms on the metal; (*c*) one H and one OH on Gr and the same water fragments on the metal; (*d*) all H and OH on Gr or (*e*) all H and OH on the substrate. Our calculations indicate that the configurations (*d*) and (*e*), where all fragments are on Gr or on Ni, are less energetically favorable by about 1.5 eV than the first reaction path leading to hydrogenation of Gr and OH chemisorption on the Ni surface. Moreover, the (*b*) and (*c*) configurations are less favorable than the (*a*), although only by 0.2 eV. Thus, our DFT calculations confirm that the most energetically favorable reaction path for the decomposition of two water molecules intercalated below Gr/Ni(111) will provide hydrogenated Gr and hydroxyl groups bonded to the substrate. As shown in Figure 3, for defect-free Gr this process is endothermic. However, the presence of Stone-Wales defects decreases the chemisorption energy and the molecular dissociation becomes exothermic. Thus, the role of the Stone-Wales defects is to increase the chemical reactivity of Gr, as it has been predicted to occurr in the hydrogenation of free-standing Gr. [41]

Then, we have evaluated the stability of the H atoms on Gr with respect to the migration to the underlying metal substrate by modelling a two-stage process: desorption of first (Figure 3c) and, successively, of the second (Figure 3d) H atom. For defect-free Gr or for Gr with a low density of Stone-Wales defects, the migration to the substrate of even a single hydrogen atom is exothermic.

This result is somehow unexpected, since the presence of an odd number of monovalent species chemisorbed on Gr should be energetically unfavorable with respect to the presence of an even number of monovalent species.[42] The destabilization in the chemical bond consequent to single-atom desorption is compensated through the occurrence of charge transfer from the substrate,[43] which makes the H migration to the metal substrate energetically convenient.

When increasing the density of Stone-Wales defects at the surface, the permanence of both H atoms on Gr becomes definitely favorable, because of the stabilizing effect of chemisorbed species, which is proportional to the number of defects. Desorption of the second H atom from Gr (Figure 3d) is energetically favorable uniquely for defect-free Gr and only in this case the H_2 molecule spontaneously forms in the space between Gr and substrate. In the presence of defects, the migration of both hydrogen atoms to the substrate has an energy cost and, thus, the formation of H dimers on the metal substrate is unfavorable without providing external energy.

Thus, DFT calculations demonstrate that, close to the Gr grain boundaries, water molecules decompose to hydrogen and hydroxyl groups and stable hydrogenation of Gr occurs. The amount of hydrogenated Gr and the configuration of the hydrogenated patterns strongly depend on the atomic structure of Gr defects at the grain boundaries. However, the Ni substrate reduces the barrier for water decomposition by more than 0.5 eV with respect to pristine free-standing, defect-free Gr.

After the elucidation of the reaction scenario, it is mandatory to evaluate the amount of hydrogen which is possible to store at the Gr/Ni(111) interface. To this aim, we probed the species evolving from the water-dosed Gr/Ni(111) interface upon thermal annealing by temperature programmed reaction (TPR). The primary role of Gr in the H_2O dissociation was evidenced by carrying out also a parallel experiment on the bare Ni(111) surface. To avoid any possible contribution due to the H_2 background in the ultra-high vacuum (UHV) chamber, we have conducted this experiment by dosing D_2O. Gr/Ni(111) and the bare Ni(111) surfaces were exposed to saturation doses of D_2O at RT and the TPR curves were measured while heating the samples at rate of 2 K/s (Figure 4, panels a and b). In the case of Gr/Ni(111), the D_2O, D_2, O_2 and O TPR profiles shown in

Figure 4a indicate that D_2 is the unique desorbing species. The D_2 desorption peak from Gr/Ni(111) centered at 442 K, corresponding to an activation energy of ~1.0 eV, is followed by a secondary peak at 643 K, corresponding to an activation energy of ~1.6 eV. These results are in fair agreement with thermal programmed desorption experiments carried out on H-dosed Gr/Ni(111).[44]

We want to point out that it is not possible to observe the desorption of D_2O during thermal annealing of D_2O-dosed Gr/Ni(111) since the very high background signal of D_2O, arising from the large dose, makes D_2O desorption hardly discernible. On the other hand, the absence of a well-distinct desorption peak for D_2O in thermal programmed desorption is also in agreement with XPS measurements reported in Figure 2d, where the O_1 component of the O 1s core level only gradually decreases above 400 K as a function of temperature.

By contrast, D_2 production from the D_2O-dosed Ni(111) is not an effective process, as demonstrated by the vanishing D_2 TPR curve shown in Figure 4b.

To further prove the occurrence of water dissociation at the Gr/Ni(111) surface at RT, we have also conducted TPR experiments with H_2O/D_2O mixtures. In this case, the observation of HD molecules, resulting from the recombination of H and D fragments, demonstrates the RT dissociation of both H_2O and D_2O at the Gr/Ni(111) interface.

The amount of D_2 evolving from the Gr/Ni(111) interface saturated at RT with water molecules was evaluated by calibrating the D_2 TPR curve, shown in Figure 4a, with the H_2 yield from the Ni(111) surface hydrogenated at 150 K up to a H saturation coverage of 0.5 ML_{Ni}. We remind that 1 ML_{Ni} corresponds to a surface atomic density of 1.86×10^{15} atoms/cm^2. The thermal programmed desorption H_2 curve, obtained from the H/Ni(111) surface and reported in Figure 4c, shows the β_2 desorption peak at 367 K and a second peak at 320 K related to the β_1 states.[45] By using the integrated intensities of this curve to normalize the D_2 TPR curve of Figure 4a, it results that the amount of D_2 evolving from water-saturated Gr/Ni(111) corresponds to 0.17 ML_{Gr} ($1ML_{Gr}=2ML_{Ni}$). From the quantitative analysis of the TPR data, we can thus assert that the gravimetric density of the hydrogenated Gr reachable in water-dosed Gr/Ni(111) interfaces is 1.42 wt.% at RT and in UHV

conditions. As a comparison, $LaNi_5$, a typical metal alloy forming hydrides, shows a gravimetric density of 1.37 wt. % [46] at RT. It is expected that decoration of Gr by Ca[47] or transition-metal atoms[48] and, moreover, the substitutional doping of Gr by N[48] or B[49] could further increase the gravimetric capacity.

Conclusions

By means of a combination of advanced spectroscopic techniques and theory, we have elucidated the mechanism leading to water decomposition at the Gr/metal interfaces at RT, resulting in hydrogenated Gr, with a gravimetric density competitive with current technology for H storage. Molecular hydrogen is produced by heating above 400 K. Our results represent a crucial milestone in the technological road map for the use of Gr/metal interfaces in catalysis and in energy-related applications.

Methods

Sample growth

The sample was a Ni(111) single crystal. The substrate was cleaned by repeated cycles of ion sputtering and annealing at 1050 K. Gr growth was carried out by dosing ethylene with the sample kept at 790 K, while monitoring in real time the C 1s line-shape (SI, Figure S1). The Gr overlayer quality is good, as indicated by the intense spots recorded in the He-atom diffraction pattern (SI, Figure S2).

Spectroscopic investigations were performed in four different UHV chambers in Trieste, Padova, Rende, and Madrid.

Exposure to water

Water was dosed at RT on a Gr/Ni(111) surface through a doser. The doser is a Mo tube with diameter 6 mm, placed almost in contact with the sample in order to enhance the local pressure. In these

conditions, we reached a partial water pressure of 10^{-3} mbar on the sample. We dosed water up to a total exposure of 10^6 L. Such a high dose is motivated by the low sticking coefficient of water molecules at RT on Gr/Ni(111) (see SI, section S3)

X-ray photoelectron spectroscopy (XPS)

High-resolution XPS experiments were performed in the UHV chamber of the SuperESCA beam line of the synchrotron radiation source Elettra (Trieste, Italy). High-resolution C 1s and O 1s core-level spectra were measured at a photon energy of 400 and 650 eV, respectively, with an overall energy resolution ranging from 40 to 150 meV. Valence-band spectra were acquired with a photon energy of 135 eV. For each spectrum, the binding energy was calibrated with the Fermi level position of the Ni substrate. The measurements were performed with the photon beam impinging at grazing incidence (70°), while photoelectrons were collected at normal emission angle. The core-level spectra were best fitted with Doniach-Šunjić functions convoluted with Gaussians, and a linear background.

High-resolution electron energy loss spectroscopy (HREELS)

HREELS experiments were performed by using an electron energy loss spectrometer (Delta 0.5, SPECS) at University of Calabria, Rende (CS), Italy. The energy resolution of the spectrometer is 5 meV. The primary electron beam energy is 4 eV. Each spectrum was normalized to the intensity of the elastic peak. HREELS spectra were acquired in specular conditions, with incident and scattering angles of 55° with respect to the surface normal.

Temperature-programmed reaction (TPR)

TPR was measured with a HIDEN HAL 301 PIC quadrupole mass spectrometer with an electron multiplier detector at University of Padova, Italy. To analyze the desorption species coming only from the sample surface, the quadrupole filter, covered by a quartz shield holding a 8 mm hole in correspondence to the sample, was placed at 5 mm from the Ni(111) single crystal, which was mounted on two tantalum wires. A linear heating ramp of 2 K/s was used. The base pressure during the experiments was better than $6 \cdot 10^{-10}$ mbar.

DFT calculations

We used DFT, as implemented in the pseudopotential code SIESTA.[50] All calculations were performed using the generalized gradient approximation (GGA-PBE) with spin-polarization[51] and implementation of the correction of van der Waals forces.[52] All calculations were carried out with an energy mesh cut-off of 360 Ry and a k-point mesh of 8×6×2 in the Monkhorst-Pack scheme.[53]

We used a rectangular supercell of 48 carbon atoms over metallic slab containing four layers (24 Ni atoms in each layer). During the optimization, the ion cores were described by norm-conserving non-relativistic pseudo-potentials[53] with cut-off radii 1.14, 1.45, 1.25, 2.15 a.u. for C, O, H and Ni, respectively, and the wave-functions were expanded with localized orbitals and double-ζ basis set for hydrogen and a double-ζ plus polarization basis set for other species. Full optimization of the atomic positions was performed. Optimization of the force and total energy was carried out with an accuracy of 0.04 eV/Å and 1 meV, respectively.

For modelling grain boundaries between Gr domains, we used Gr with different amount of Stone-Wales defects (see Fig 3a). The intercalation energy was calculated by:

$E_{intercalation} = E_{system+2H2O} - (E_{system} + 2E_{H2O})/m$

where E_{system} and $E_{system+2H2O}$ are the total energy of Gr on metallic substrate before and after the intercalation of two water molecules, respectively; E_{H2O} is the total energy of water molecule and m is the number of carbon atoms in the supercell.

The optimized distance between the metal substrate and Gr obtained in our calculations agrees with experimental values in literature (see discussion in Ref. 54).

Associated content

The Supporting Information (SI) is available free of charge on the ACS Publications website.

The SI reports additional experiments on real-time growth of Gr on Ni(111), the evaluation of the crystalline quality of the grown Gr layer by He-atom scattering (HAS) and of the cticking coefficient of water on Gr/Ni(111) at RT. Moreover, it reports vibrational experiments on Ice formation and desorption in Gr/metals and more details the analysis of the high-resolution C 1s spectra. The last two

sections of SI report calculations of core-level shifts and more details on the DFT model on water dissociation at RT in Gr/metals.

.

Acknowledgments

AP and GC thank Fabio Vito for technical support. AP and RL thank Elettra Sincrotrone Trieste S.C.p.A. for financial support. RL acknowledges the support by MIUR through the program "Progetto Premiale 2012" - Project ABNANOTECH. SA, MC and GG acknowledge Italian MIUR through the national grant Futuro in Ricerca 2012 RBFR128BEC "Beyond graphene: tailored C-layers for novel catalytic materials and green chemistry" and by the University of Padova funded project: CPDA128318/12 "Study of the catalytic activity of complex graphene nanoarchitectures from ideal to real conditions". DF acknowledges European Union (FP7): Theme NMP.2012.1.4-3 Grant no. 309672. Calculations are partially supported by the Ministry of Education and Science of the Russian Federation, Project no. 16.1751.2014/K.

Author information

The authors declare no competing financial interests.

REFERENCES

1. Satyapal, S.; Petrovic, J.; Read, C.; Thomas, G.; Ordaz, G., The U.S. Department of Energy's National Hydrogen Storage Project: Progress towards meeting hydrogen-powered vehicle requirements. *Catal. Today* **2007,** *120*, 246-256.
2. McAteer, D.; Gholamvand, Z.; McEvoy, N.; Harvey, A.; O'Malley, E.; Duesberg, G. S.; Coleman, J. N., Thickness Dependence and Percolation Scaling of Hydrogen Production Rate in MoS_2 Nanosheet and Nanosheet–Carbon Nanotube Composite Catalytic Electrodes. *ACS Nano* **2016,** *10*, 672–683.
3. Duan, J.; Chen, S.; Jaroniec, M.; Qiao, S. Z., Porous C_3N_4 Nanolayers@N-Graphene Films as Catalyst Electrodes for Highly Efficient Hydrogen Evolution. *ACS Nano* **2015,** *9*, 931-940.
4. Fan, X.; Peng, Z.; Ye, R.; Zhou, H.; Guo, X., M_3C (M: Fe, Co, Ni) Nanocrystals Encased in Graphene Nanoribbons: An Active and Stable Bifunctional Electrocatalyst for Oxygen Reduction and Hydrogen Evolution Reactions. *ACS Nano* **2015,** *9*, 7407-7418.

5. Ting, V. P.; Ramirez-Cuesta, A. J.; Bimbo, N.; Sharpe, J. E.; Noguera-Diaz, A.; Presser, V.; Rudic, S.; Mays, T. J., Direct Evidence for Solid-like Hydrogen in a Nanoporous Carbon Hydrogen Storage Material at Supercritical Temperatures. *ACS Nano* **2015,** *9*, 8249-8254.
6. Liguras, D. K.; Kondarides, D. I.; Verykios, X. E., Production of hydrogen for fuel cells by steam reforming of ethanol over supported noble metal catalysts. *Appl. Catal., B: Environ.* **2003,** *43*, 345-354.
7. Das, D.; Veziroğlu, T. N., Hydrogen production by biological processes: a survey of literature. *Int. J. Hydrogen Energy* **2001,** *26*, 13-28.
8. Cortright, R. D.; Davda, R. R.; Dumesic, J. A., Hydrogen from catalytic reforming of biomass-derived hydrocarbons in liquid water. *Nature* **2002,** *418*, 964-967.
9. Kim, M.-S.; Baek, J.-S.; Yun, Y.-S.; Jun Sim, S.; Park, S.; Kim, S.-C., Hydrogen production from Chlamydomonas reinhardtii biomass using a two-step conversion process: Anaerobic conversion and photosynthetic fermentation. *Int. J. Hydrogen Energy* **2006,** *31*, 812-816.
10. Doyle, R. L.; Godwin, I. J.; Brandon, M. P.; Lyons, M. E. G., Redox and electrochemical water splitting catalytic properties of hydrated metal oxide modified electrodes. *Phys. Chem. Chem. Phys.* **2013,** *15*, 13737-13783.
11. Bak, T.; Nowotny, J.; Rekas, M.; Sorrell, C. C., Photo-electrochemical hydrogen generation from water using solar energy. Materials-related aspects. *Int. J. Hydrogen Energy* **2002,** *27*, 991-1022.
12. Kment, S.; Schmuki, P.; Hubicka, Z.; Machala, L.; Kirchgeorg, R.; Liu, N.; Wang, L.; Lee, K.; Olejnicek, J.; Cada, M.; Gregora, I.; Zboril, R., Photoanodes with Fully Controllable Texture: The Enhanced Water Splitting Efficiency of Thin Hematite Films Exhibiting Solely (110) Crystal Orientation. *ACS Nano* **2015,** *9*, 7113-7123.
13. Chen, Y.; Tran, P. D.; Boix, P.; Ren, Y.; Chiam, S. Y.; Li, Z.; Fu, K.; Wong, L. H.; Barber, J., Silicon Decorated with Amorphous Cobalt Molybdenum Sulfide Catalyst as an Efficient Photocathode for Solar Hydrogen Generation. *ACS Nano* **2015,** *9*, 3829-3836.
14. Steier, L.; Luo, J.; Schreier, M.; Mayer, M. T.; Sajavaara, T.; Grätzel, M., Low-Temperature Atomic Layer Deposition of Crystalline and Photoactive Ultrathin Hematite Films for Solar Water Splitting. *ACS Nano* **2015,** *9*, 11775-11783.
15. Tozzini, V.; Pellegrini, V., Prospects for hydrogen storage in graphene. *Phys. Chem. Chem. Phys.* **2013,** *15*, 80-89.
16. Bonaccorso, F.; Colombo, L.; Yu, G.; Stoller, M.; Tozzini, V.; Ferrari, A. C.; Ruoff, R. S.; Pellegrini, V., Graphene, related two-dimensional crystals, and hybrid systems for energy conversion and storage. *Science* **2015,** *347*, 1246501.
17. Balog, R.; Andersen, M.; Jørgensen, B.; Sljivancanin, Z.; Hammer, B.; Baraldi, A.; Larciprete, R.; Hofmann, P.; Hornekær, L.; Lizzit, S., Controlling Hydrogenation of Graphene on Ir(111). *ACS Nano* **2013,** *7*, 3823–3832.
18. Kumar, R.; Oh, J.-H.; Kim, H.-J.; Jung, J.-H.; Jung, C.-H.; Hong, W. G.; Kim, H.-J.; Park, J.-Y.; Oh, I.-K., Nanohole-Structured and Palladium-Embedded 3D Porous Graphene for Ultrahigh Hydrogen Storage and CO Oxidation Multifunctionalities. *ACS Nano* **2015,** *9*, 7343-7351.
19. Sakintuna, B.; Lamari-Darkrim, F.; Hirscher, M., Metal hydride materials for solid hydrogen storage: A review. *Int. J. Hydrogen Energy* **2007,** *32*, 1121-1140.
20. Jena, P., Materials for Hydrogen Storage: Past, Present, and Future. *J. Phys. Chem. Lett.* **2011,** *2*, 206-211.
21. Murray, L. J.; Dinca, M.; Long, J. R., Hydrogen storage in metal-organic frameworks. *Chem. Soc. Rev.* **2009,** *38*, 1294-1314.

22. Politano, A.; Chiarello, G., Periodically rippled graphene on Ru(0001): A template for site-selective adsorption of hydrogen dimers via water splitting and hydrogen-spillover at room temperature. *Carbon* **2013,** *61*, 412-417.
23. Politano, A.; Marino, A. R.; Formoso, V.; Chiarello, G., Water adsorption on graphene/Pt(111) at room temperature: A vibrational investigation. *AIP Advances* **2011,** *1*, 042130.
24. Patera, L. L.; Africh, C.; Weatherup, R. S.; Blume, R.; Bhardwaj, S.; Castellarin-Cudia, C.; Knop-Gericke, A.; Schloegl, R.; Comelli, G.; Hofmann, S.; Cepek, C., In Situ Observations of the Atomistic Mechanisms of Ni Catalyzed Low Temperature Graphene Growth. *ACS Nano* **2013,** *7*, 7901-7912.
25. Zhao, W.; Kozlov, S. M.; Höfert, O.; Gotterbarm, K.; Lorenz, M. P. A.; Viñes, F.; Papp, C.; Görling, A.; Steinrück, H.-P., Graphene on Ni(111): Coexistence of Different Surface Structures. *J. Phys. Chem. Lett.* **2011,** *2*, 759-764.
26. Grüneis, A.; Kummer, K.; Vyalikh, D. V., Dynamics of graphene growth on a metal surface: A time-dependent photoemission study. *New J. Phys.* **2009,** *11*, 073050.
27. Ng, M. L.; Balog, R.; Hornekær, L.; Preobrajenski, A. B.; Vinogradov, N. A.; Mårtensson, N.; Schulte, K., Controlling Hydrogenation of Graphene on Transition Metals. *J. Phys. Chem. C* **2010,** *114*, 18559-18565.
28. Yamamoto, S.; Bluhm, H.; Andersson, K.; Ketteler, G.; Ogasawara, H.; Salmeron, M.; Nilsson, A., In situ x-ray photoelectron spectroscopy studies of water on metals and oxides at ambient conditions. *J. Phys.: Condens. Matter* **2008,** *20*, 184025.
29. Weser, M.; Rehder, Y.; Horn, K.; Sicot, M.; Fonin, M.; Preobrajenski, A. B.; Voloshina, E. N.; Goering, E.; Dedkov, Y. S., Induced magnetism of carbon atoms at the graphene/Ni(111) interface. *Appl. Phys. Lett.* **2010,** *96*, 012504.
30. Böttcher, S.; Weser, M.; Dedkov, Y.; Horn, K.; Voloshina, E.; Paulus, B., Graphene on ferromagnetic surfaces and its functionalization with water and ammonia. *Nanoscale Res. Lett.* **2011,** *6*, 214.
31. Hunt, A.; Dikin, D. A.; Kurmaev, E. Z.; Boyko, T. D.; Bazylewski, P.; Chang, G. S.; Moewes, A., Epoxide Speciation and Functional Group Distribution in Graphene Oxide Paper-Like Materials. *Adv. Funct. Mater.* **2012,** *22*, 3950-3957.
32. Kim, H.; Balgar, T.; Hasselbrink, E., The stretching vibration of hydrogen adsorbed on epitaxial graphene studied by sum-frequency generation spectroscopy. *Chem. Phys. Lett.* **2011,** *508*, 1-5.
33. Henderson, M. A., The interaction of water with solid surfaces: fundamental aspects revisited. *Surf. Sci. Rep.* **2002,** *46*, 1-308.
34. Politano, A.; Chiarello, G.; Benedek, G.; Chulkov, E. V.; Echenique, P. M., Vibrational measurements on alkali coadsorption systems: experiments and theory. *Surf. Sci. Rep.* **2013,** *68*, 305–389.
35. Elias, D. C.; Nair, R. R.; Mohiuddin, T. M. G.; Morozov, S. V.; Blake, P.; Halsall, M. P.; Ferrari, A. C.; Boukhvalov, D. W.; Katsnelson, M. I.; Geim, A. K.; Novoselov, K. S., Control of graphene's properties by reversible hydrogenation: Evidence for graphane. *Science* **2009,** *323*, 610-613.
36. Feng, X.; Maier, S.; Salmeron, M., Water splits epitaxial graphene and intercalates. *J. Am. Chem. Soc.* **2012,** *134*, 5662–5668.
37. Petrović, M.; Šrut Rakić, I.; Runte, S.; Busse, C.; Sadowski, J. T.; Lazić, P.; Pletikosić, I.; Pan, Z. H.; Milun, M.; Pervan, P.; Atodiresei, N.; Brako, R.; Šokčević, D.; Valla, T.; Michely, T.; Kralj, M., The mechanism of caesium intercalation of graphene. *Nat. Commun.* **2013,** *4*, 2772.
38. Yao, Y.; Fu, Q.; Zhang, Y. Y.; Weng, X.; Li, H.; Chen, M.; Jin, L.; Dong, A.; Mu, R.; Jiang, P.; Liu, L.; Bluhm, H.; Liu, Z.; Zhang, S. B.; Bao, X., Graphene cover-promoted metal-catalyzed reactions. *Proc. Natl. Acad. Sci., U. S. A.* **2014**.
39. Jin, L.; Fu, Q.; Dong, A.; Ning, Y.; Wang, Z.; Bluhm, H.; Bao, X., Surface Chemistry of CO on Ru(0001) under the Confinement of Graphene Cover. *J. Phys. Chem. C* **2014,** *118*, 12391–12398.

40. Wei, M.; Fu, Q.; Yang, Y.; Wei, W.; Crumlin, E.; Bluhm, H.; Bao, X., Modulation of Surface Chemistry of CO on Ni(111) by Surface Graphene and Carbidic Carbon. *J. Phys. Chem. C* **2015,** *119*, 13590-13597.
41. Boukhvalov, D. W.; Katsnelson, M. I., Chemical Functionalization of Graphene with Defects. *Nano Lett.* **2008,** *8*, 4373-4379.
42. Galakhov, V. R.; Buling, A.; Neumann, M.; Ovechkina, N. A.; Shkvarin, A. S.; Semenova, A. S.; Uimin, M. A.; Yermakov, A. Y.; Kurmaev, E. Z.; Vilkov, O. Y.; Boukhvalov, D. W., Carbon States in Carbon-Encapsulated Nickel Nanoparticles Studied by Means of X-ray Absorption, Emission, and Photoelectron Spectroscopies. *J. Phys. Chem. C* **2011,** *115*, 24615-24620.
43. Boukhvalov, D. W.; Son, Y. W.; Ruoff, R. S., Water Splitting over Graphene-Based Catalysts: Ab Initio Calculations. *ACS Catalysis* **2014,** *4*, 2016-2021.
44. Zhao, W.; Gebhardt, J.; Späth, F.; Gotterbarm, K.; Gleichweit, C.; Steinrück, H.-P.; Görling, A.; Papp, C., Reversible Hydrogenation of Graphene on Ni(111)—Synthesis of "Graphone". *Chem. Eur. J.* **2015,** *21*, 3347-3358.
45. Russell, J. N.; Gates, S. M.; Yates, J. T., Isotope effects in hydrogen adsorption on Ni(111): Direct observation of a molecular precursor state. *J. Chem. Phys.* **1986,** *85*, 6792-6802.
46. Schlapbach, L.; Züttel, A., Hydrogen-storage materials for mobile applications. *Nature* **2001,** *414*, 353-358.
47. Lee, H.; Ihm, J.; Cohen, M. L.; Louie, S. G., Calcium-Decorated Graphene-Based Nanostructures for Hydrogen Storage. *Nano Lett.* **2010,** *10*, 793-798.
48. Parambhath, V. B.; Nagar, R.; Ramaprabhu, S., Effect of Nitrogen Doping on Hydrogen Storage Capacity of Palladium Decorated Graphene. *Langmuir* **2012,** *28*, 7826-7833.
49. Beheshti, E.; Nojeh, A.; Servati, P., A first-principles study of calcium-decorated, boron-doped graphene for high capacity hydrogen storage. *Carbon* **2011,** *49*, 1561-1567.
50. Soler, J. M.; Artacho, E.; Gale, J. D.; García, A.; Junquera, J.; Ordejón, P.; Sánchez-Portal, D., The SIESTA method for ab initio order- N materials simulation. *J. Phys.: Condens. Matter* **2002,** *14*, 2745.
51. Perdew, J. P.; Burke, K.; Ernzerhof, M., Generalized Gradient Approximation Made Simple. *Phys. Rev. Lett.* **1996,** *77*, 3865-3868.
52. Román-Pérez, G.; Soler, J. M., Efficient Implementation of a van der Waals Density Functional: Application to Double-Wall Carbon Nanotubes. *Phys. Rev. Lett.* **2009,** *103*, 096102.
53. Troullier, N.; Martins, J. L., Efficient pseudopotentials for plane-wave calculations. *Phys. Rev. B* **1991,** *43*, 1993-2006.
54. Boukhvalov, D. W.; Gornostyrev, Y. N.; Uimin, M. A.; Korolev, A. V.; Yermakov, A. Y., Atomic, electronic and magnetic structure of graphene/iron and nickel interfaces: theory and experiment. *RSC Advances* **2015,** *5*, 9173-9179.

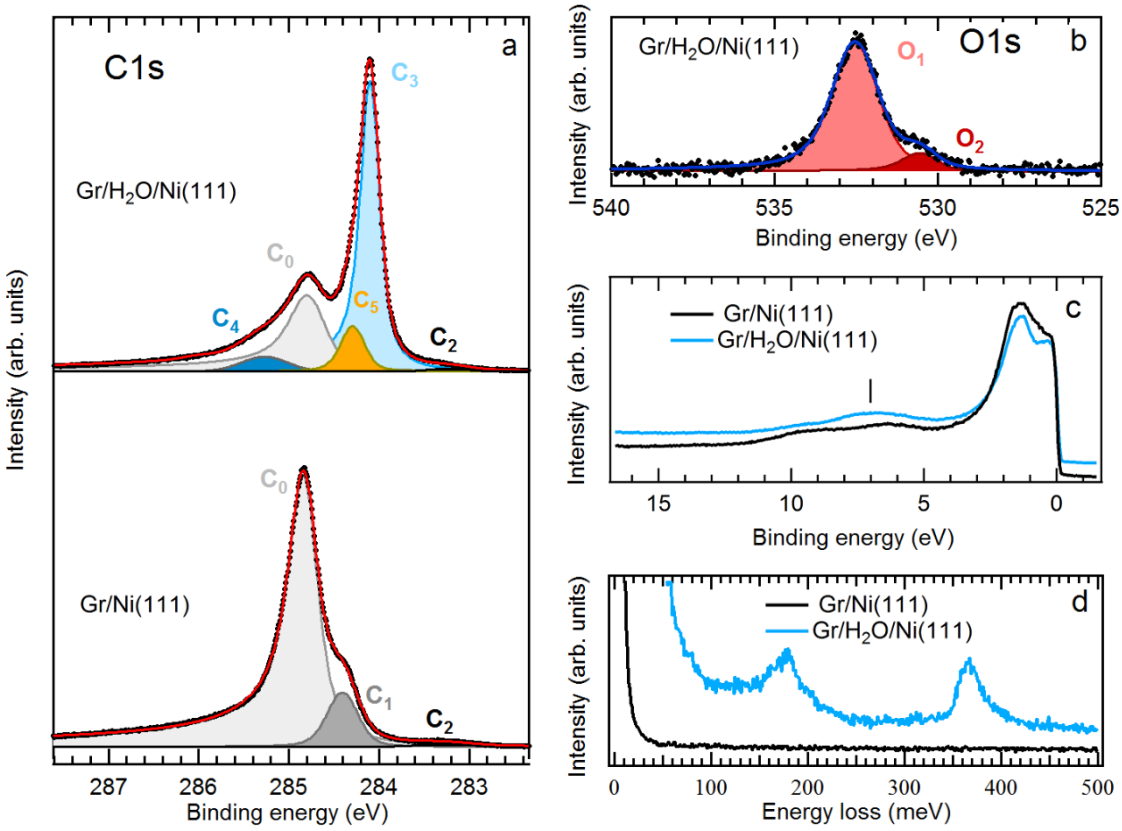

Figure 1. XPS and vibrational investigation of pristine and water-exposed Gr. (a) C 1s core-level spectra in pristine Gr/Ni(111) (top panel) and H_2O-exposed Gr/Ni(111) (bottom panel), measured with photon energy of 400 eV. The assignment of the various components is described in the main text. **(b)** O 1s core-level spectrum in H_2O-exposed Gr/Ni(111). The photon energy is 650 eV. **(c)** Valence-band spectra in pristine (black curve) and H_2O-expoxed Gr/Ni(111) (blue curve). Spectra have been shifted for clarity. The photon energy is 135 eV. **(d)** Vibrational spectrum, measured by HREELS in specular scattering conditions for pristine (black curve) and H_2O-expoxed Gr/Ni(111) (blue curve). The primary electron beam energy is 4 eV.

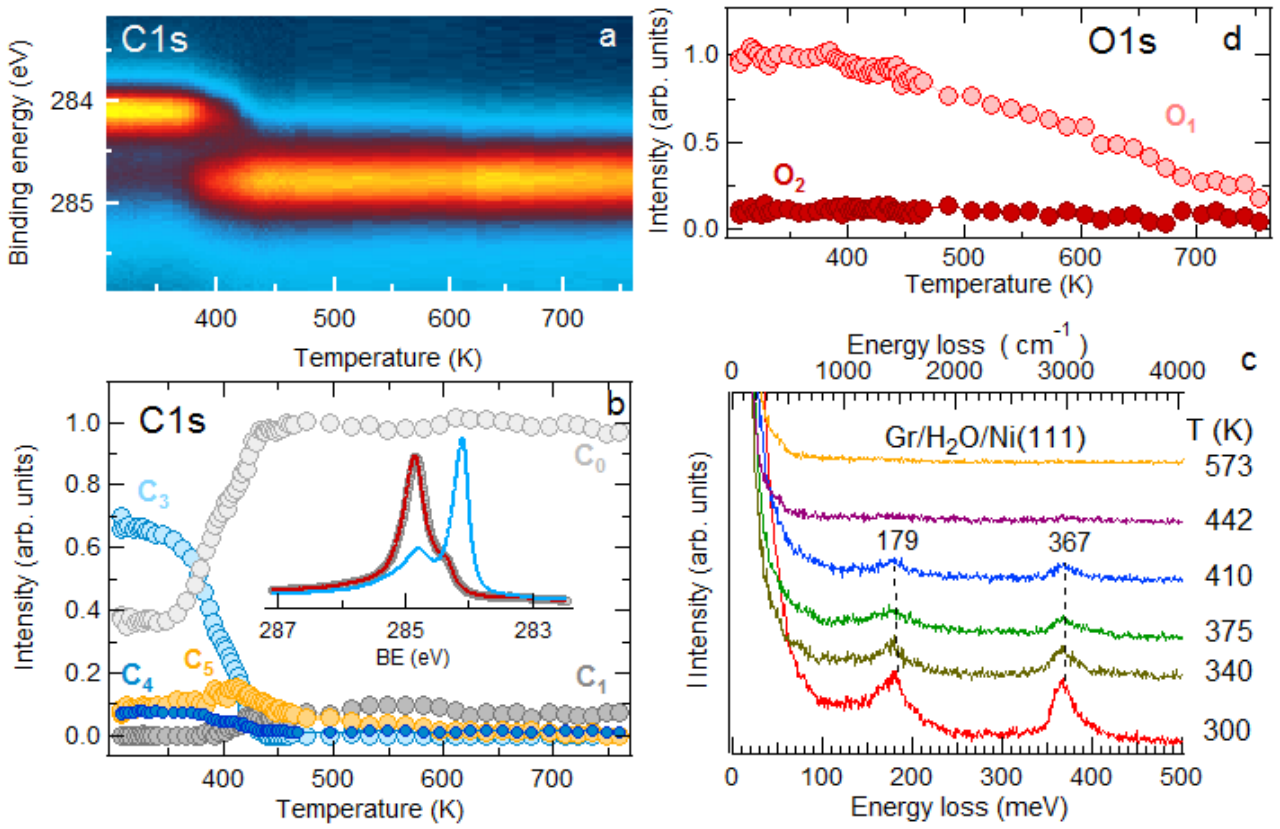

Figure 2. Desorption of water fragments from Gr. (a) Real-time evolution of the C 1s signal in H_2O-exposed Gr/Ni(111) during the heating at a rate of 0.4 K/s. **(b)** Intensity of the various components of the C 1s core-level spectrum. Each peak has been labeled as in Figure 1a. The inset shows the C 1s signal recorded for Gr/Ni(111) (grey circles), H_2O-dosed Gr/Ni(111) (red curve) and after heating to 442 K (blue curve). **(c)** Vibrational spectrum measured by HREELS for the H_2O-modified Gr/Ni(111) surface, annealed to different values of temperature. The bottom axis reports vibrational energies in meV, while the corresponding values in cm^{-1} are shown in the top axis. **(d)** Intensity of the O_1 and O_2 components (see Figure 1b) in O 1s spectra recorded in real time during the heating of the water-exposed Gr/Ni(111) interface from 300 up to 750 K. The intensities have been obtained by fitting the O 1s spectra with two Voigt line-shapes after background subtraction.

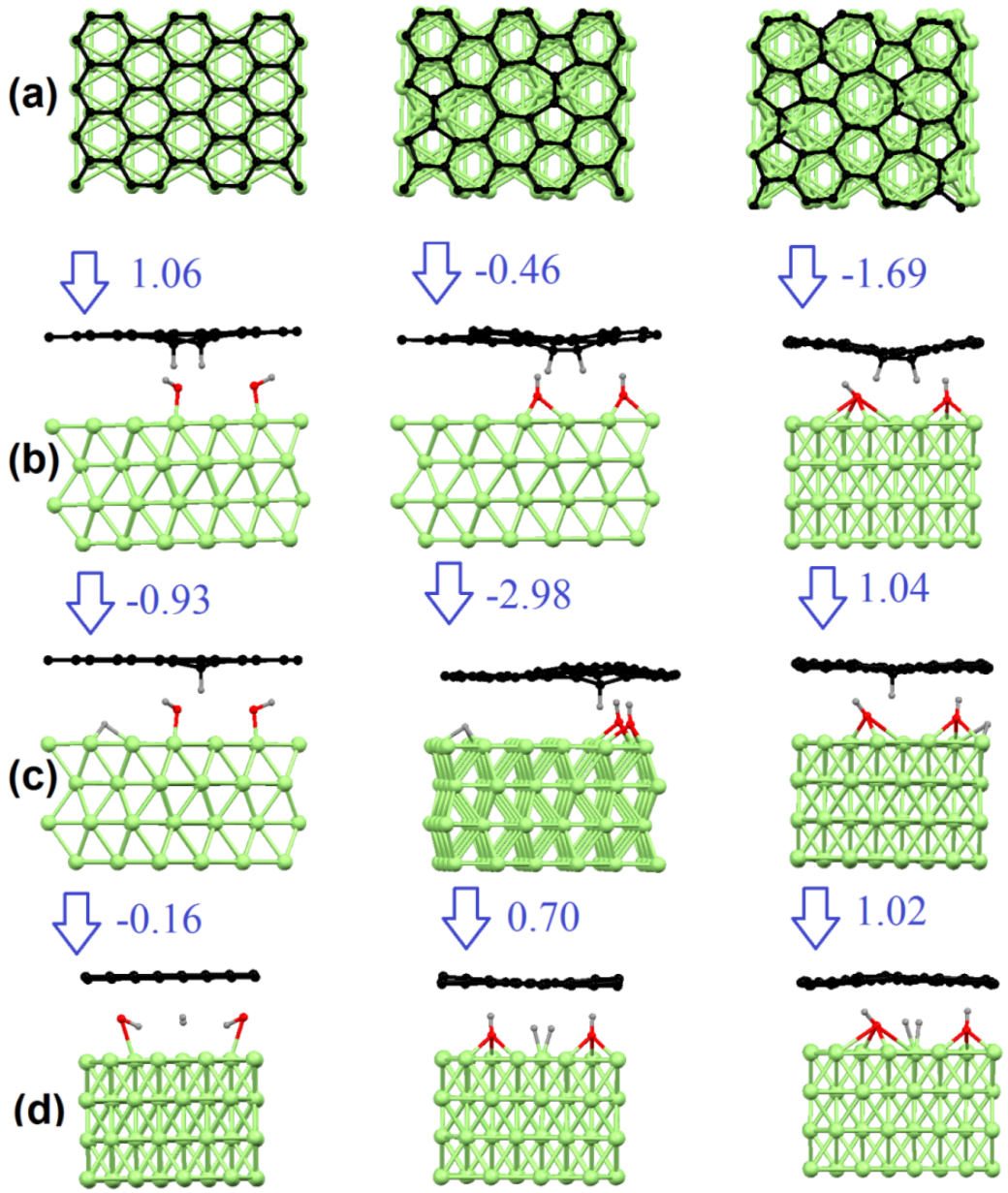

Figure 3. DFT model on water-induced hydrogenation of Gr/metals. Optimized atomic structures of Gr without (left column) and with various amount of defects (central and right columns) for: **(a)** Gr/Ni(111); **(b**) intercalation of two water molecules, which decompose into hydroxyl groups bonded to the Ni substrate and hydrogen atoms covalently bonded to Gr; migration of one **(c)** and two **(d)** hydrogen atoms from Gr to the metal substrate. Numbers correspond to the energetic values (in eV) of the various processes.

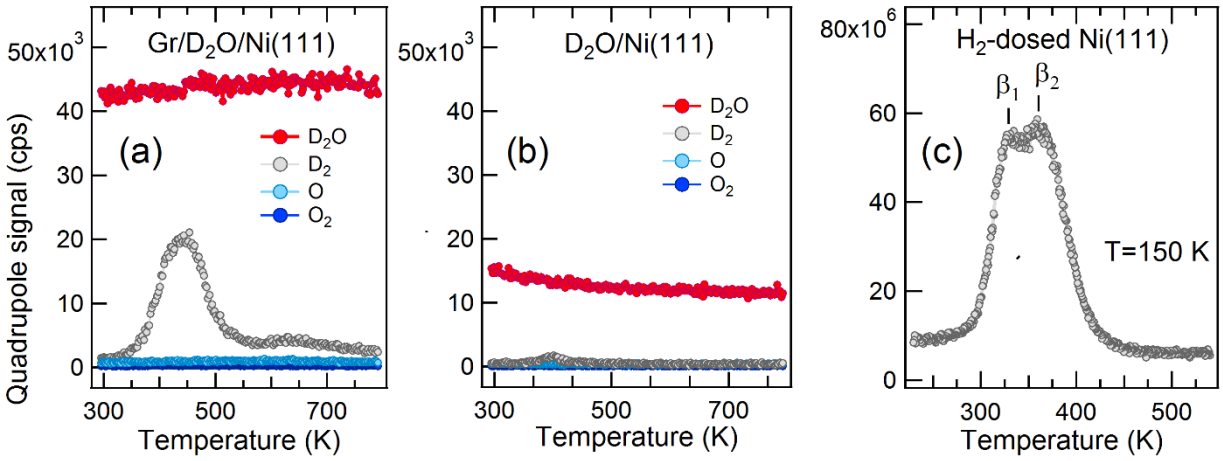

Figure 4. D_2 production from D_2O. TPR spectra acquired for the D_2O-exposed Gr/Ni(111) and Ni(111) surfaces are reported in panels **(a)** and **(b)**, respectively. The evolution of D_2O (red circles), D_2 (grey circles), atomic O (pale blue circles) and O_2 (dark blue circles) has been recorded. The weak D_2 desorption peak from Ni(111) is caused by residual deuterium in the water flask. **(c)** Thermal programmed desorption spectra of the H_2-dosed Ni(111) surface acquired using a 2 K/s heating rate.